ORIGINAL PAPER

An effective interaction in polypyrrole/nickel phosphide (PPy/Ni$_2$P) for high-performance supercapacitor

Shuling Liu[1,2] (ORCID) · Yan Chen[1,2] · Jing Ren[1,2] · Yueyan Wang[1,2] · Wei Wei[1,2]

Abstract

Polypyrrole/nickel phosphide (PPy/Ni$_2$P) composites were synthesized through a facile two-step method. The results show that when there is 30% Ni$_2$P in PPy/Ni$_2$P (active material 3 mg), the prepared composites possess uniform morphology, which composed of large quantities of broccoli-like PPy microstructures (average dimension of about 200 nm) and Ni$_2$P spherical particles (average diameters of 250 nm). It achieves a higher specific capacity for 476.5 F g^{-1} at a current density of 1 A g^{-1} in a three-electrode system, even after 3000 cycles the capacity maintained 89%. The excellent electrochemical performance of PPy/Ni$_2$P composites may be due to the good dispersion and uniform morphology of Ni$_2$P nanoparticles. In addition, the synergistic effect between PPy and Ni$_2$P nanoparticles also dramatically improves the electrochemical properties of the composites.

Keywords Polypyrrole · Nickel phosphide · Supercapacitor · Electrochemical performance

Introduction

Supercapacitors, also known as ultracapacitors, have been extensively researched as an attractive power solution for electronic devices, hybrid vehicles, and energy storage applications due to their high specific capacitance, fast charge and discharge process, and excellent stability during long-term cycling [1–4]. Nevertheless, its practical application suffers from the lack of high-performance electrode materials available, especially those obtained through a facile synthesis or at a lower production cost. Therefore, seeking ideal electrode material has been the research focus in recent study. Nowadays, three primary categories of electrode materials for supercapacitors have been explored: (1) carbon materials (activated carbon and graphene) [5, 6], (2) transition metal oxides (MnO$_2$ and Fe$_2$O$_3$) [7, 8], (3) conductive polymers (polyaniline, or polypyrrole) [9, 10].

Many efforts have been committed to researching these conductive polymers, such as polyethylenedioxythiophene (PEDOT), polyaniline (PANI), and polypyrrole (PPy). PPy becomes a promising candidate for supercapacitor electrode materials owning to its high electric conductivity, large specific capacitance [11, 12], fine processability, conveniences of preparation, and low cost of monomer [13]. Nevertheless, PPy is unsteadiness during the consecutive charge/discharge processes, which leads to its mechanical degradation and poor electrochemical performances [14–16]. To address this problem, other materials were frequently combined with polypyrrole to form composites, which possess enhanced specific capacitance and mechanical and electrical properties. For example, Tsai et al. manufactured graphene/PPy composite by means of electrochemical polymerization, which possesses high specific capacitance of 352 F g^{-1} at a current density of 1 A g^{-1} [15]. Pispas et al. reported the PPy/non-covalent graphene composite via electrodeposition polymerization with a higher specific capacitance of 383 F g^{-1} at 0.5 A g^{-1} [17]. Compared with other components, nickel phosphide (Ni$_2$P) has its unique difference. It is one of interstitial compounds that have special crystal structure, which endow them high active site and high electronic conductivity [18, 19]. Besides, it can deliver higher capacity and better stability owing to smaller volume expansion [20–22]. However, the poor cycle stability always limits its application and leads to less capacitance [23, 24]. Therefore, building PPy/Ni$_2$P composites might be a good choice to improve the electrochemical performances of PPy or Ni$_2$P by their interaction between them.

✉ Shuling Liu
shulingliu@aliyun.com

1   College of Chemistry and Chemical Engineering, Shaanxi University of Science and Technology, Xi'an 710021, China

2   Shaanxi Key Laboratory of Chemical Additives for Industry, Xi'an 710021, China

Herein, in the present study, to bring fully the advantages of PPy or Ni_2P monomer, the PPy/Ni_2P composites with different mass ratios (10%, 20%, 30%, 40% Ni_2P) were successfully prepared by a two-step method. It was found that the electrochemical performance of as-prepared PPy/Ni_2P composite can be greatly enhanced when the mass ratio between PPy and Ni_2P is 30%. Its specific capacitance can reach up to 476.5 F g^{-1} at the current density of 1 A g^{-1} and its capacitance maintains 89% even after 3000 cycles.

Experimental section

Pyrrole (C_4H_5N, AR, Shanghai Aladdin Biochemical Technology Co., Ltd), P-hydroxybenzene sulfonate sodium ($C_4H_7NaO_5S$, AR, Shanghai McLean Biochemical Technology Co., Ltd), ammonium persulfate (($NH_4)_2S_2O_8$, AR, Tianjin Tianli Chemical Reagent Co., Ltd), anhydrous sodium sulfate(Na_2SO_4, AR, Tianjin Tianli Chemical Reagent Co., Ltd), white phosphorus (P_4,AR, Hongyan Chemical Reagent Factory, Hedong District, Tianjin), N-methyl pyrrolidone (C_5H_9NO, AR, National Medicine Group Chemical Reagent Co., Ltd), polyvinylidene fluoride (-[-$C_2H_2F_2$-]$_n$-, AR, National Medicine Group Chemical Reagent Co., Ltd), acetylene black (C, AR, Tianjin Kemiou Chemical Reagent Co., Ltd), absolute ethyl alcohol (C_2H_5OH, AR, Tianjin Tianli Chemical Reagent Co., Ltd), deionized water (H_2O).

Synthesis of nickel phosphide (Ni_2P) nanoparticles

In a typical experimental procedure, an appropriate amount of hexadecyltrimethylammonium bromide (CTAB, 0.1 g) and $NiCl_2 \cdot 6H_2O$ (0.237 g, 1 mmol) were dissolved in distilled water until a uniform solution was formed. This solution was stirred further for 1 h at room temperature. The resulting solution was transferred into a 50-mL Teflon-lined autoclave, and then, white phosphorous (WP, 2 mmol, 0.237 g) was added. The mixed solution was heated at 180 °C for 16 h. Then, the autoclave was cooled down to room temperature. The as-obtained products were filtered and further washed via benzene, absolute ethanol, and distilled water to remove the impurities. The as-obtained products were dried in a vacuum at 60 °C for 6 h and then collected.

Synthesis of PPy/Ni_2P composites

The different amount of as-obtained Ni_2P nanoparticles dispersed uniformly in the distilled water. Then, the Py monomer (0.33 g, 4.9 mmol) and sodium p-hydroxybenzene sulfonate (0.322 g, 1.3 mmol, as dopant) were added to above solution under an ice bath and stirring. After agitating for 30 min, the

ammonium persulfate (2.248 g, 9.8 mmol, APS) was slowly added into the solution, and the polymerization reaction proceeded in the ice bath for 24 h. The obtained black PPy/Ni_2P composites were washed by distilled water and absolute ethyl alcohol respectively to remove impurities, and then dried at 60 °C for 12 h in a vacuum oven. The as-prepared PPy/Ni_2P composites were collected for further characterization. The other composites with different mass ratios of PPy/Ni_2P are named as PPy/Ni_2P (10%), PPy/Ni_2P (20%), and PPy/Ni_2P (40%), respectively.

Characterization

The phase and structure of the sample were detected by X-ray diffraction (XRD, Rigaku-S4800, Japan), the morphology of the sample was observed with a field emission scanning electron microscope (FE-SEM Hitachi S-4800, Japan), and the elements were analyzed by an energy-dispersive X-ray feature (EDS, Hitachi S-4800, Japan), The surface area of the product was calculated from N_2 adsorption/desorption isotherms at 77 K that were conducted on an analyzer (BET, Gemini VII 2390, America), the electrochemical properties (cyclic voltammetry, galvanostatic charge and discharge, and AC impedance) were measured on a Parstat MC electrochemical workstation (Princeton PARSTATMC, America) by making use of three-electrode system in the presence of 1 mol L^{-1} Na_2SO_4 as electrolyte. The PPy or PPy/Ni_2P composite was used as the working electrode, and a platinum plate and a saturated calomel electrodes (SCEs) as the counter and reference electrodes, respectively.

Electrochemical measurements

The electrochemical performance of the as-obtained electrode materials was tested on a electrochemical workstation (Princeton PARSTATMC, America). Working electrodes were prepared by mixing as-obtained active material (80 wt.%), acetylene black (10 wt.%), and polyvinylidene fluoride (PVDF, 10 wt.%), coating on a piece of foamed nickel. The electrochemical measurements were carried out in a three-electrode system with platinum electrode as counter electrode and a saturated calomel electrode (SCE) as the reference electrodes, respectively. The cyclic voltammogram (CV), galvanostatic charge-discharge (GCD) (with a voltage range from −0.4 to 0.4 V) and the electrochemical impedance spectroscopy (EIS) (in the frequency range of 0.01–100,000 Hz with perturbation amplitude of 5 mV at open circuit potential) were carried out in 1 M Na_2SO_4 aqueous solution using CHI660E electrochemical workstation (Shanghai Chen Hua) at room temperature.

Results and discussion

Structure and morphology

SEM images of PPy, Ni_2P, and PPy/Ni_2P complexes with different loading weights are shown in Fig. 1. As can be seen from Fig. 1a, bare PPy has a cauliflower-like structure with the particle size of about 200 nm, the surface is rough and slightly agglomerated. Figure 1 b shows the image pure Ni_2P, which consists of agglomerated spherical particles with various sizes. Figure 1 c–f show the PPy/Ni_2P composites with different loadings (10%, 20%, 30%, and 40%) of Ni_2P. Among them, Fig. 1 c is PPy/Ni_2P (10%); large quantities of cauliflower-like PPy are presented in the composite, while few Ni_2P spherical particles are shown, probably due to the loading of Ni_2P is low. Figure 1 d and f show the PPy/Ni_2P (20%) and PPy/Ni_2P (40%), respectively. Different from PPy/Ni_2P (10%), large quantities of Ni_2P spherical particles with a smooth surface present with PPy exists as cauliflower-like structure, demonstrating that the composite material formed. However, obvious agglomeration occurs, which is detrimental to their electrochemical performance. Figure 1 e shows the PPy/Ni_2P (30%) composite. A large number of homogeneous Ni_2P spherical particles with the diameter about 200 nm are uniformly dispersed on the surface of PPy. High specific surface area microstructure is desirable in the electrode material, for it can not only facilitate the penetration of the electrolyte but also provide an effective path for charge transfer, eventually could greatly improve the specific capacity.

Fig. 2 a and b show the typical XRD patterns of PPy cauliflowers, Ni_2P nanoparticles, and PPy/Ni_2P composites. From curve a of Fig. 2a, all of the diffraction peaks can be

corresponded to the pure hexagonal phase of Ni_2P, which is close to the standard values (JCPDS No.: 74-1385). The diffraction peaks are narrow and sharp, and no peaks from other phases such as NiO, Ni_3P, and Ni_5P_4 are observed, suggesting its good crystalline nature. Curve b of pure PPy exhibits a broad diffraction peak located at $2\theta = 25°$, indicating the amorphous characteristic of cauliflower-like PPy [25] nanostructures. Curve c of PPy/Ni_2P composite is similar to curve b, and it also manifests a broad diffraction peak at $2\theta = 25°$. What's more, no any diffraction peaks ascribed to hexagonal structure Ni_2P nanoparticles are detected owning to its weak crystallinity and small amount, which indicates that the synthetic procedure of PPy/Ni_2P composites lowers greatly the crystallinity of Ni_2P nanoparticles. Moreover, the diffraction peak intensity of PPy/Ni_2P composites decreases with the amount of Ni_2P nanoparticles increasing (10%, 20%, 30%, 40%). Fig. 2 c–f are the corresponding EDS spectra of four PPy/Ni_2P composites (10%, 20%, 30%, 40%), which are used to further investigate the formation of Ni_2P nanostructures in the composites. The results show that all four PPy/Ni_2P composites are composed of C, O, S, N, Ni, and P elements. C, O, Ni, and P elements are derived from PPy/Ni_2P composites, suggesting the appearance of Ni_2P nanoparticles. Also, the amounts of Ni and P elements are increasing gradually and the amounts of C, O, S, and N are decreasing from the inset data of Fig. 2c–f, while S element can be aligned to the adding of sodium phydroxybenzenesulfonate, which is used as the doping agent to provide sulfonic acid ions to polymerize polypyrrole monomer.

The FT-IR spectra of PPy [26], Ni_2P, and PPy/Ni_2P composites are described in Fig. 3a. Among them, curves a and b describe the corresponding FT-IR spectra of Ni_2P (curve a)
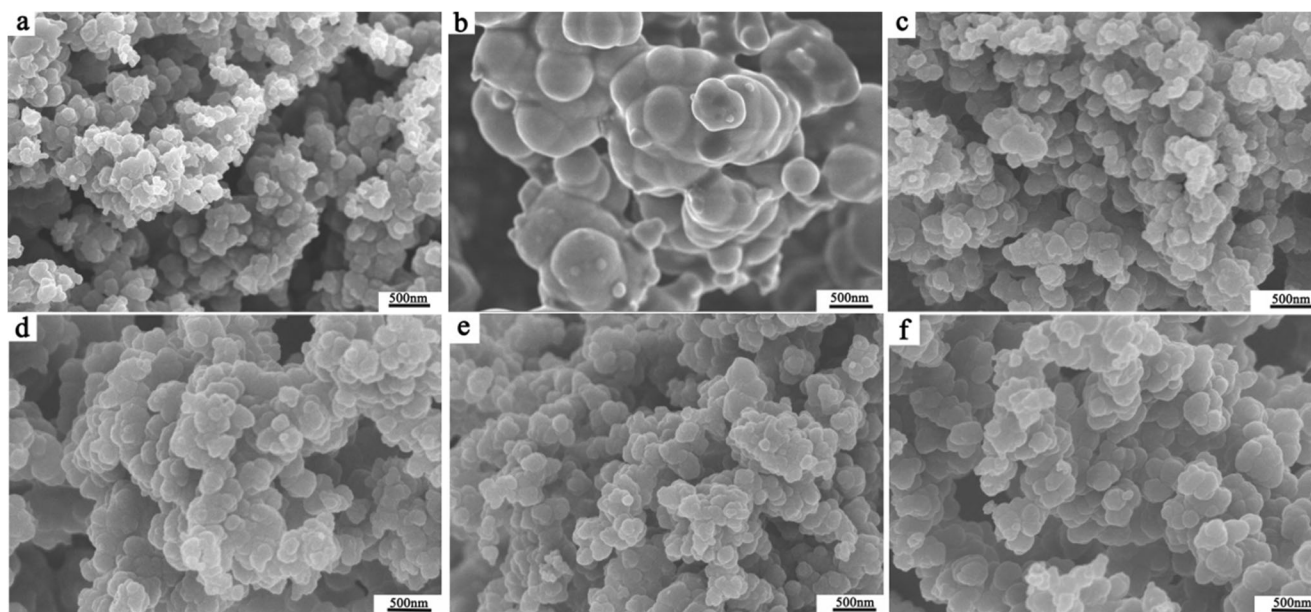

Fig. 1 SEM images of **a** PPy, **b** Ni_2P, **c** PPy/Ni_2P (10%), **d** PPy/Ni_2P (20%), **e** PPy/Ni_2P (30%), and **f** PPy/Ni_2P (40%) composites
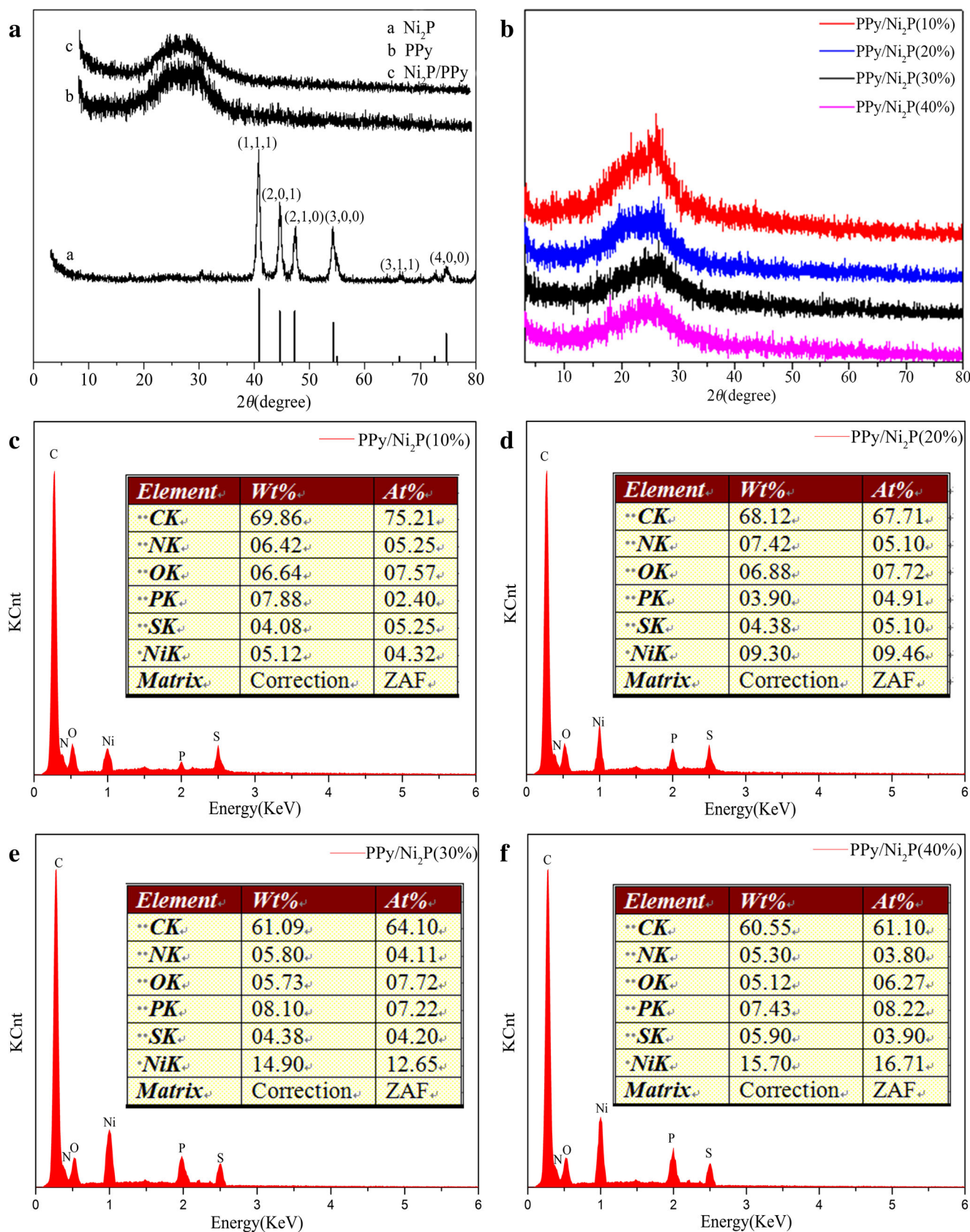
Fig. 2 XRD patterns of **a** Ni$_2$P, PPy, and PPy/Ni$_2$P composites and **b** different PPy/Ni$_2$P (10%, 20%, 30%, 40%) composites. EDS spectra of **c** PPy/Ni$_2$P (10%), **d** PPy/Ni$_2$P (20%), **e** PPy/Ni$_2$P (30%), and **f** PPy/Ni$_2$P (40%)
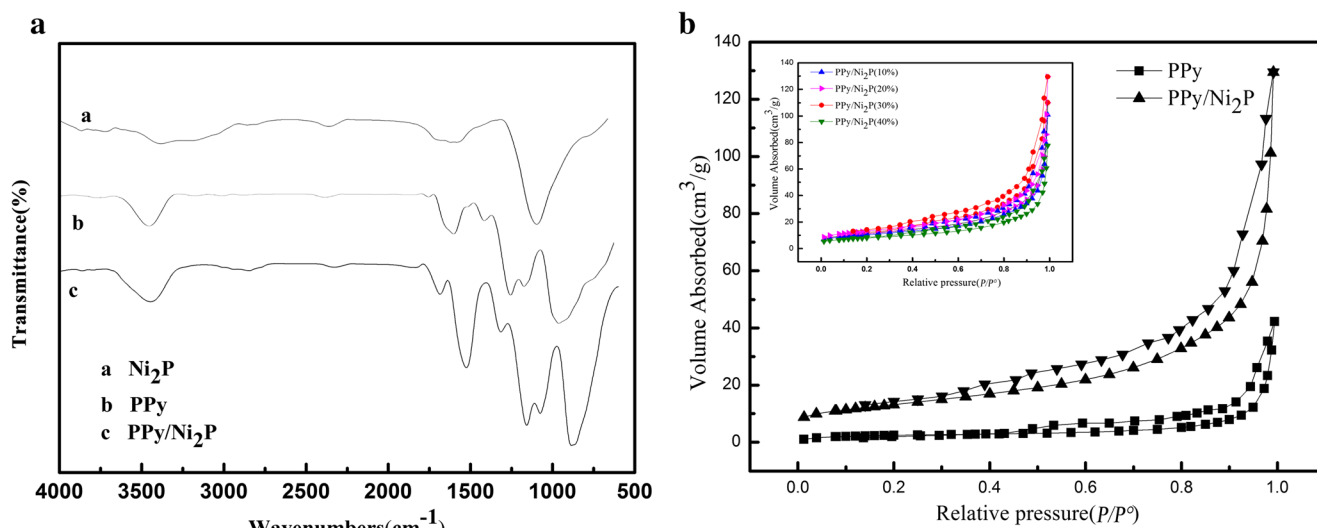
a

b

Fig. 3 **a** FT-IR spectra of Ni_2P, PPy, and PPy/Ni_2P composites and **b** nitrogen adsorption-desorption isotherms of PPy and PPy/Ni_2P (30%) composites

and PPy (curve b), respectively. The characterized peak of Ni_2P nanoparticles in curve a appears at around 1100 cm^{-1}. And this characterized peak intensity in PPy/Ni_2P composite has a modest decrease by comparing three curves, indicating PPy/Ni_2P composite has been prepared successfully. In addition, the appearance of a new broad absorption band at around 1305 cm^{-1} (curve c) and the change in peak intensity and position also suggest that there is a good interaction between PPy and Ni_2P nanostructures, which seems to imply a good electrochemical performance. Figure 3 b shows the N_2 adsorption-desorption isotherms of the as-obtained PPy and PPy/Ni_2P composite electrodes at 77 K. The N_2 adsorption-desorption isotherms suggest that PPy and PPy/Ni_2P composites have similar pore structures. However, it is worth noting that the surface area of PPy/Ni_2P (30%) composites (72.29 m^2 g^{-1}) is much higher than that of PPy/Ni_2P (10%) composite (65.51 m^2 g^{-1}), PPy/Ni_2P (20%) composite (68.98 m^2 g^{-1}), PPy/Ni_2P (40%) composite (70.82 m^2 g^{-1}), and PPy nanostructures (27.01 m^2 g^{-1}). This result might be due to the contribution of PPy nanostructures adhered to the surface of Ni_2P nanoparticles, which enhanced surface area–contributing voids between adjacent Ni_2P nanoparticles [26].

Electrochemical performances

The electrochemical performance of the as-obtained electrode materials is evaluated by CV, GCD, and AC impedance (EIS) in a three-electrode system in 1 mol dm^{-3} Na_2SO_4 aqueous solution. Figure 4 a shows the CV curves of PPy and PPy/Ni_2P composite electrodes at the scan rate of 10 mV s^{-1} between −0.4 and 0.4 V (vs SCE). Obviously, the CV curves of as-prepared PPy/Ni_2P electrodes exhibit quasi-rectangular shape compared with PPy, which demonstrates a good capacitive behavior owing to the simultaneous contribution of

faradaic and non-faradaic redox reactions in a neutral electrolyte. Furthermore, no major redox peaks are found from CV curves, indicating that no irreversible reactions have occurred and also suggesting high stability of the PPy/Ni_2P composite electrodes [27]. Moreover, the specific capacitance of PPy/Ni_2P (30%) is also optimum among four composite electrodes. The reason might be the larger specific surface areas of PPy/Ni_2P electrodes and good interaction between PPy and Ni_2P nanostructures, which are more beneficial to promote ion diffusion and store charges. Especially for PPy/Ni_2P (30%), the good interaction endows it larger specific surface area based on the quasi-rectangular shape area. Figure 4 b shows the CV curves of PPy/Ni_2P (30%) composite at different scan rates ranging from 2 to 10 mV s^{-1}. All these CV curves show relatively rectangular shapes [28], which indicates that PPy/Ni_2P (30%) composite exhibits good capacitance performance even at different scan rates. The reason might be that Ni_2P has an interstitial structure, which endows it higher active sites and higher electronic conductivity, which is better for ion transferring. Also, there exists a good interaction, and this better interaction effect between PPy and Ni_2P microstructures greatly increases ion storage chance and ion diffusion, which can gain more access to almost all available pores of the electrode materials [29]. Further, the PPy/Ni_2P (30%) composite has the largest specific surface area and can provide more surface area–contributing voids between adjacent Ni_2P nanoparticles, which is helpful for the electrochemical performances when used as supercapacitor electrodes. The GCD curves of PPy and PPy/Ni_2P composites are presented in Fig. 4c at the current density of 1 A g^{-1} within a potential between −0.4 and 0.4 V. It can be obviously observed that the almost linear and nearly symmetric charging-discharging curves verify good capacitive behavior and good electrochemical reversibility. Moreover, PPy/Ni_2P composites possess longer galvanostatic
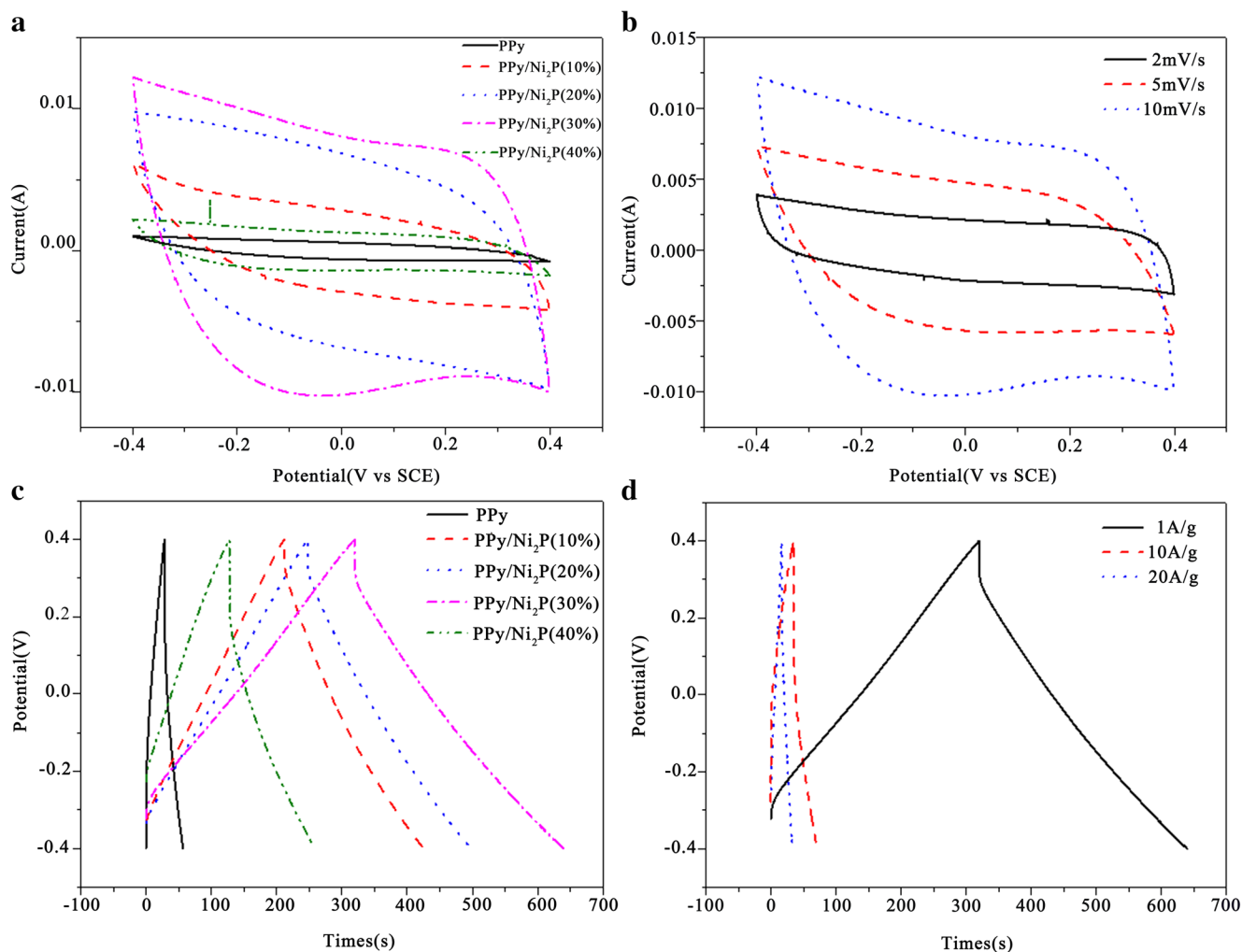
Fig. 4 **a** CV curves of PPy and PPy/Ni$_2$P composites at the rate of 10 mV s^{-1}. **b** CV curves of PPy/Ni$_2$P(30%)composite at different scan rates. **c** Galvanostatic charge-discharge curves (GCD) of PPy and PPy/ Ni$_2$P composites at the current density of 1 A g^{-1}. **d** Galvanostatic charge-discharge curves of PPy/Ni$_2$P(30%) at different current densities

charge-discharge times than PPy. The longer charging/ discharging periods for PPy/Ni$_2$P composites indicate the enhancement of pseudocapacitive behavior. What's more, the charging/discharging times of PPy/Ni$_2$P composites first become longer with the increment of Ni$_2$P (10%, 20%, 30%), but then begin to shorten when Ni$_2$P achieves to 40%. Therefore, the electrochemical performance of PPy/Ni$_2$P (30%) composites is the best, which is consistent with the CV results. Figure 4 d shows the triangular-shaped galvanostatic charge/discharge curves of PPy/Ni$_2$P (30%) composite at different current densities from 1 to 20 A g^{-1}. The charge-discharge times of PPy/Ni$_2$P (30%) composite decrease with the current density increasing, which is mainly be ascribed to the common concentration polarization phenomenon during the electrochemical reactions. And, the charge-discharge curves are close to the isosceles triangle and the charge curves are symmetrical with the discharge curves, which indicates that the electrochemical reactions of PPy/Ni$_2$P (30%) composite have good reversible performance.

The specific capacitances of the PPy/Ni$_2$P composite at current densities are shown in Fig. 5a. The specific capacitance is calculated by formula (1) [30].

$$Cs = \frac{I\Delta t}{m\Delta V} \tag{1}$$

As observed from Fig. 5a, the specific capacitances of all electrodes decrease with the increment of the current densities from 1 to 50 A g^{-1}. At the current density of scan rate of 1 A g^{-1}, the specific capacitance of PPy/Ni$_2$P (30%) composite is about 476.5 F g^{-1}, which is higher than those of 262.5 F g^{-1} for PPy/Ni$_2$P (10%), 312 F g^{-1} for PPy/Ni$_2$P (20%), and 196.5 F g^{-1} for PPy/Ni$_2$P (40%). The poor interactions between PPy and Ni$_2$P in PPy/Ni$_2$P (10%) and PPy/Ni$_2$P (20%) for insufficient Ni$_2$P microstructures and smaller surface area of PPy/Ni$_2$P (40%) might be related to the above results obtained at different scan rates and current densities. When further increasing to a higher current density of 50 A g^{-1}, the specific capacitance of all PPy/Ni$_2$P electrodes decreases.
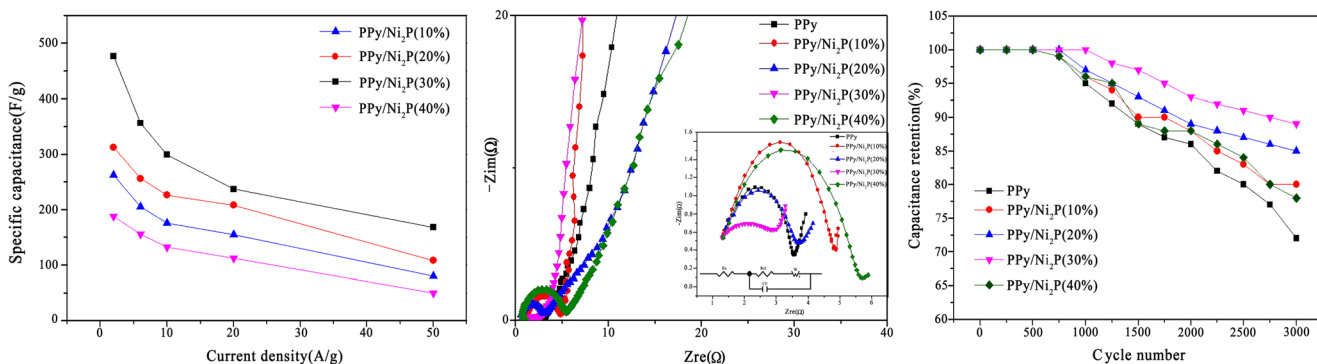
Fig. 5 **a** Specific capacitance of PPy/Ni$_2$P (10%), PPy/Ni$_2$P (20%), PPy/Ni$_2$P (30%), and PPy/Ni$_2$P (40%). **b** Nyquist plots of PPy and PPy/Ni$_2$P composites. **c** Long-term cycling performances of PPy and PPy/Ni$_2$P composites at the current density of 1 A g^{-1}

This might be that the higher current density causes some structure collapse of the composites and decreases the interaction between PPy and Ni$_2$P nanostructures. But obviously, the specific capacitance of PPy/Ni$_2$P (30%) is still the largest, which can reach to 168 F g^{-1}, while those of PPy/Ni$_2$P (10%), PPy/Ni$_2$P (20%), and PPy/Ni$_2$P (40%) are 80 F g^{-1}, 108 F g^{-1}, and 51 F g^{-1}, respectively. Except that, the electrochemical impedance measurements (EIS) were also performed to explore the difference of the as-obtained PPy and PPy/Ni$_2$P composite electrodes (Fig. 5b). The inset shows the equivalent fitted circuit. Normally, a semicircle in the high-frequency can be corresponded to the charge-transfer resistance (R_{ct}) associated with the double-layer capacitance, that is, the charge transfer at the exposure interface between electrode and electrolyte. The larger the semicircle is, the higher the charge-transfer resistance is. As observed from the corresponding Nyquist plots, the charge-transfer resistances of PPy/Ni$_2$P are higher than those of PPy. Their charge-transfer resistances are 5.5 for PPy, 2.5 for PPy/Ni$_2$P (10%), 2.2 for PPy/Ni$_2$P (20%), 1.8 for PPy/Ni$_2$P (30%), and 3.5 Ω for PPy/Ni$_2$P (40%), respectively. And PPy/Ni$_2$P (30%) possesses the least charge-transfer resistance. The smaller charge-transfer resistance signifies a faster kinetics process of electrode [31]; therefore, the electrochemical reactions of PPy/Ni$_2$P composite electrode are easier to happen compared with PPy. The straight line with certain slope at lower frequency (Warburg impedance W) is associated with the mass-transfer resistance of electrodes, which is the characteristic of the capacitive behavior [32]. The larger the angle between the line and the abscissa has, the smaller the mass-resistance has, which represents ideal capacitance performance; from the comparison, the angle of PPy/Ni$_2$P (30%) is the largest, which indicates that PPy/Ni$_2$P (30%) has the best capacitance performance.

The cycle stability of PPy and PPy/Ni$_2$P composite electrodes is also investigated by GCD test between −0.4 and 0.4 V at the current density of 1 A g^{-1} and the results are shown in Fig. 5c. As shown from Fig. 5c, the specific capacitances of PPy and the PPy/Ni$_2$P composite electrodes keep about 72%, 80%, 85%, 89%, and 78% of its initial capacitance

after 3000 cycles respectively, indicating the good cycle stability of PPy/Ni$_2$P composites. Again, the cycling stability of PPy/Ni$_2$P (30%) composite electrode is the best. The good cycling performance is probably due to the synergistic effect between PPy and Ni$_2$P, which produce more pore structures for effective charge transfer and fast electrolyte diffusion. Furthermore, the presence of Ni$_2$P in composites can increase the mechanical strength of composites and prevent swelling and shrinking of PPy during the charging-discharging process, which is helpful for improving not only the capacitance but also the cycling performance of the electrodes.

In addition, the capacitances of reported supercapacitors fabricated using polypyrrole composites are summarized in Table 1 (tested in three-electrode systems). The electrochemical performance of the polypyrrole composites reported in this paper are among the best.

The loading weight is also an important parameter for the electrochemical performance of active material. Therefore, PPy/Ni$_2$P (30%) composite electrode was chosen to investigate the optimum loading weight at 1 A g^{-1} (Fig. 6). The above loading weight of PPy and PPy/Ni$_2$P (30%) composite electrodes is kept at 3 mg. Obviously observed from Fig. 6a, the largest CV area is achieved indicating the best capacitance, which is consistent with the above CV result PPy/Ni$_2$P (30%). When the loading weight changes to 1, 5, and 7 mg, the CV area would decrease. Also from the galvanostatic charge-

Table 1 Capacitance comparison of different PPy-based electrodes (three-electrode system) for the supercapacitor application

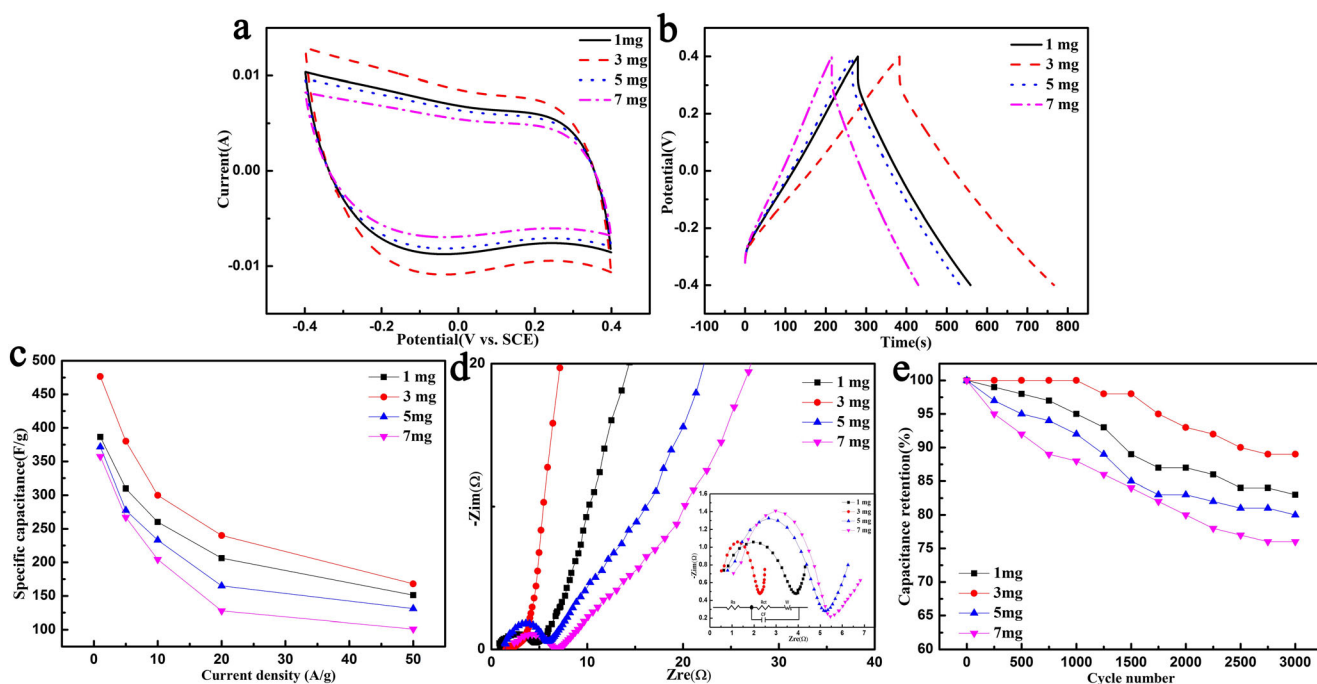| Work electrode	Cs (F/g)	Current (A/g)	Electrolyte	Ref
MnO$_3$/PPy	129	1	1 M Na$_2$SO$_4$	[34]
MnO$_2$/PPy	205	1	1 M Na$_2$SO$_4$	[35]
CNTs/PPy	282	1	1 M KCl	[36]
GO/PPy	302.6	1	1 M Na$_2$SO$_4$	[37]
PANI/PPy	350	1	1 M H$_2$SO$_4$	[38]
MnMoO$_4$/PPy	313	1	2 M KCl	[39]
PPy/Ni$_2$P	476.5	1	1 M Na$_2$SO$_4$	This work

Fig. 6 **a** CV curves of PPy and PPy/Ni$_2$P composites at the rate of 10 mV s^{-1}. **b** Galvanostatic charge-discharge curves of PPy/Ni$_2$P(30%)with different loadings at the current density of 1 A g^{-1}. **c** Specific capacitance of PPy/Ni$_2$P (30%) with different loadings at different current densities. **d** Nyquist plots of PPy/Ni$_2$P composites with different loadings. **e** Long-term cycling performances of PPy/Ni$_2$P (30%) composites with different loadings at the current density of 1 A g^{-1}

discharge curve of PPy/Ni$_2$P (30%) (Fig. 6b), PPy/Ni$_2$P (30%) possesses the longest charge-discharge time when the loading weight is 3 mg. The reason may be that the much higher loading weight would increase impedance, which leads to the poor electrochemical properties. While the lower loading weight would produce inevitable measurement error. The value of specific capacitance at different current densities can be seen from Fig. 6c. The specific capacitance of PPy/Ni$_2$P composite decreases with the current density increasing, which is mainly attributed to the fact that it is hard for the electrolyte ions to access the interior surfaces of the electroactive materials at high current density [33].

Nyquist plots of PPy/Ni$_2$P (30%) composites with different loadings are shown in Fig. 6d; the inset shows the equivalent circuit used to fit the data, which consists of an equivalent series resistance (R_s) and a charge-transfer resistance (R_{ct}). The semicircles of EIS data suggest that R_{ct} of PPy/Ni$_2$P (30%) composite electrodes are 3.4 (1 mg), 1.8 (3 mg), 4.4 (5 mg), and 4.1 Ω (7 mg), respectively, and R_s values are 0.71, 0.55, 0.80, and 1.10 Ω, respectively. The R_{ct} and R_s for the 3-mg loading weight are the lowest, which rooting from its good conductivity, demonstrating the preferable charge-transfer ability at the interface of electrode/electrolyte of PPy/Ni$_2$P (30%) with the loading weight is 3 mg [40, 41]. In addition, the low-frequency region (Warburg impedance W) of the PPy/Ni$_2$P (30%) composite at 3 mg loading weight has the largest slope, suggesting that the ionic diffusion is accelerated, corresponding to its better capacitive behavior. This character

is also a direct result of the fast diffusion and quick adsorption of ions from the solution onto the electrode surface. Thus, the loading weight can affect some electrochemical activities during the electrochemical reactions process, and fast ion diffusion and low charge-transfer resistance play key roles for good and utilization of as-obtained PPy and PPy/Ni$_2$P (30%) composite electrodes. Fig. 6 e investigates the cycling stability of PPy/Ni$_2$P (30%) at a current density of 1 A g^{-1} and in the potential range from − 0.4 to 0.4 V. After 3000 cycles, PPy/Ni$_2$P (30%) with 3-mg loading weight possesses 89% of its initial capacitance, while other only 83%, 80%, and 74% left. The enhanced cycle stability for the 3-mg loading weight can be ascribed to the strong interaction between PPy and Ni$_2$P. This result further indicates that PPy/Ni$_2$P (30%) has good electrochemical performance when the loading weight is 3 mg.

Conclusions

The different PPy/Ni$_2$P composites were successfully prepared by a facile two-step process. The PPy/Ni$_2$P composites are composed of two components, cauliflower-like PPy and spherical Ni$_2$P microstructures. The good interaction between PPy and Ni$_2$P gives the as-prepared composites enhanced electrochemical performance, which posses a larger specific capacitance (476.5 F g^{-1}) at current density of 1 A g^{-1} and good cycling stability being up to 89% after 3000 cycles when used as supercapacitor electrode. Herein, the preparation of PPy/Ni$_2$P

composites can not only provide an idea for new supercapacitor electrode design also widen their application range.

References

1. Reddy ALM, Amitha FE, Jafri I, Ramaprabhu S (2008) Asymmetric flexible supercapacitor stack. Nanoscale Res Lett 3(4):145–151

2. Patil SJ, Bulakhe RN, Lokhande CD (2015) Nanoflake-modulated La2Se3 thin films prepared for an asymmetric supercapacitor device. Chempluschem 80(9):1478–1487

3. Shen KW, Ran F, Zhang XX, Liu C, Wang NJ, Niu XQ et al (2015) Supercapacitor electrodes based on nano-polyaniline deposited on hollow carbon spheres derived from cross-linked co-polymers. Synth Met 209:369–376

4. Xiong T, Lee WSV, Chen L, Tan TL, Huang XL, Xue JM (2017) Indole-based conjugated macromolecules as a redox-mediated electrolyte for an ultrahigh power supercapacitor. Energy Environ. Sci. 10(11):2441–2449

5. Candelaria SL, Shao YY, Zhou W, Li XL, Xiao J, Zhang JG et al (2012) Nanostructured carbon for energy storage and conversion. Nano Energy 1(2):195–220

6. Zhao J, Wang ZY, Zhao Q, Xing BS (2014) Adsorption of phenanthrene on multilayer graphene as affected by surfactant and exfoliation. Environmental Science & Technology 48(1):331–339

7. Tack LW, Azam MA, Seman R (2017) Structural and electronic properties of transition-metal oxides attached to a single-walled CNT as a lithium-ion battery electrode: a first-principles study. J Phys Chem A 121(13):2636–2642

8. Zhang SL, Guan BY, Wu HB, Lou XWD (2018) Metal-organic framework-assisted synthesis of compact Fe_2O_3 nanotubes in Co_3O_4 host with enhanced lithium storage properties. Nano-Micro Letters 10(3)

9. Cabrera L, Gutierrez S, Morales MP, Menendez N, Herrasti P (2009) Magnetic conducting composites based on polypyrrol and iron oxide nanoparticles synthesized via electrochemistry. J Magn Magn Mater 321(14):2115–2120

10. Dong YT, Feng JX, Li GR (2017) Transition metal ion-induced high electrocatalytic performance of conducting polymer for oxygen and hydrogen evolution reactions. Macromol Chem Phys 218(22)

11. Gao Y, Ding K, Xu X, Wang YZ, Yu DM (2014) PPy film/TiO_2 nanotubes composite with enhanced supercapacitive properties (vol 4, pg 27130, 2014). RSC Adv 4(77): 40898–40898

12. Wang JP, Wu CJ, Wu PQ, Li X, Zhang M, Zhu JB (2017) Polypyrrole capacitance characteristics with different doping ions and thicknesses. Phys Chem Chem Phys 19(31):21165–21173

13. Zhu Y, Shi K, Zhitomirsky I (2014) Anionic dopant-dispersants for synthesis of polypyrrole coated carbon nanotubes and fabrication of supercapacitor electrodes with high active mass loading. J Mater Chem A 2(35):14666

14. Chang HH, Chang CK, Tsai YC, Liao CS (2012) Electrochemically synthesized graphene/polypyrrole composites and their use in supercapacitor. Carbon 50(6):2331–2336

15. Zhu JB, Xu YL, Wang J, Wang JP (2012) Electropolymerization and characterization of fast charge-discharge PPy/F-SWNTs composite materials. Acta Phys -Chim Sin 28(2):373–380

16. Chabi S, Peng C, Yang Z, Xia Y, Zhu Y (2015) Three dimensional (3D) flexible graphene foam/polypyrrole composite: towards highly efficient supercapacitors. RSC Adv 5(6):3999–4008

17. Skaltsas T, Tagmatarchis N, Pispas S (2015) Non-covalent graphene/polymer functional materials. Curr Org Chem 19(18): 1800–1818

18. Cecilia JA, Infantes-Molina A, Rodríguez-Castellón E, Jiménez-López A (2009) A novel method for preparing an active nickel phosphide catalyst for HDS of dibenzothiophene. J Catal 263(1): 4–15

19. Liu S, Wang Y, Ma L, Zhang H (2018) Ni_2P/ZnS (CdS) core/shell composites with their photocatalytic performance. J Mater Res 33(21):3580–3588

20. Lu Y, Tu JP, Xiang JY, Wang XL, Zhang J, Mai YJ et al (2011) Improved electrochemical performance of self-assembled hierarchical nanostructured nickel phosphide as a negative electrode for lithium ion batteries. J.phys.chem.c 115(48): 23760-23767

21. Lu Y, Tu JP, Xiong QQ, Qiao YQ, Wang XL, Gu CD et al (2012) Synthesis of dinickel phosphide (Ni_2P) for fast lithium-ion transportation: a new class of nanowires with exceptionally improved electrochemical performance as a negative electrode. Cheminform 2(8):3430–3436

22. Nitta N, Wu F, Lee JT, Yushin G (2015) Li-ion battery materials: present and future. Mater Today 18(5):252–264

23. Li W, Wang X, Xiao X, Xu F, Sun Y, Zhuang L (2013) Reduced graphene oxide/nickel cobaltite nanoflake composites for high specific capacitance supercapacitors. Electrochim Acta 111(6):937–945

24. Shi K, Zhitomirsky I (2013) Polypyrrole nanofiber–carbon nanotube electrodes for supercapacitors with high mass loading obtained using an organic dye as a co-dispersant. J Mater Chem A 1(38): 11614–11622

25. Debiemme-Chouvy C (2009) Template-free one-step electrochemical formation of polypyrrole nanowire array. Electrochem Commun 11(2):298–301

26. Ananda SR, Murugendrappa MV (2018) Impedance study of synthesized cobalt aluminum oxide/polypyrrole nano-composites. Materials Today Proceedings 5(1):2955–2959

27. Yao T, Cui T, Wang H, Xu L, Cui F, Wu J (2014) A simple way to prepare Au@polypyrrole/Fe_3O_4 hollow capsules with high stability and their application in catalytic reduction of methylene blue dye. Nanoscale 6(13):7666–7674

28. Davies A, Audette P, Farrow B, Hassan F, Yu A (2011) Graphene-based flexible supercapacitors: pulse-electropolymerization of polypyrrole on free-standing graphene films. J Phys Chem C 115(35):17612–17620

29. LEE, Hyuck, SUK CHO MI, Kim IH, Nam JD, LEE et al (2010) RuO_x/polypyrrole nanocomposite electrode for electrochemical capacitors. Synth Met 160(9): 1055–1059

30. Yang P, Mai W (2014) Flexible solid-state electrochemical supercapacitors. Nano Energy 8(6):274–290

31. Kant R, Sarathbabu M, Srivastav S (2013) Effect of uncompensated solution resistance on quasireversible charge transfer at rough and finite fractal electrode. Electrochim Acta 95(11):237–245

32. Asen P, Shahrokhian S, Zad AI (2017) One step electrodeposition of V_2O_5/polypyrrole/graphene oxide ternary nanocomposite for preparation of a high performance supercapacitor. Int J Hydrog Energy 42(33)

33. Cheng Q, Tang J, Ma J, Zhang H, Shinya N, Qin LC (2011) Graphene and carbon nanotube composite electrodes for supercapacitors with ultra-high energy density. Physical Chemistry Chemical Physics Pccp 13(39):17615–17624

34. Zhang X, Zeng X, Yang M, Qi Y (2014) Investigation of a branchlike MoO_3/polypyrrole hybrid with enhanced electrochemical performance used as an electrode in supercapacitors. ACS Appl Mater Interfaces 6(2):1125–1130

35. Yuan L, Wan C, Zhao L (2015) Facial in-situ synthesis of MnO$_2$/PPy composite for supercapacitor. Int J Electrochem Sci 10(11):9456–9465

36. Oliveira AHPD, Oliveira HPD (2014) Carbon nanotube/ polypyrrole nanofibers core–shell composites decorated with titanium dioxide nanoparticles for supercapacitor electrodes. J Power Sources 268(4):45–49

37. Fan LQ, Liu GJ, Wu JH, Liu L, Lin JM, Wei YL (2014) Asymmetric supercapacitor based on graphene oxide/polypyrrole composite and activated carbon electrodes. Electrochim Acta 137(8):26–33

38. Wen L, Ping H, Zhang S, Dong F, Ma Y (2014) One-step triple-phase interfacial synthesis of polyaniline-coated polypyrrole composite and its application as electrode materials for supercapacitors. J Power Sources 266(1):347–352

39. Wang H, Song Y, Zhou J, Xu X, Wei H, Jing Y et al (2016) High-performance supercapacitor materials based on polypyrrole composites embedded with core-sheath polypyrrole@MnMoO 4 nanorods. Electrochim Acta 212:775–783

40. Wu Z, Guo J, Wang J, Liu R, Xiao W, Xuan C et al (2017) Hierarchically porous electrocatalyst with vertically aligned defect-rich CoMoS nanosheets for the hydrogen evolution reaction in an alkaline medium. ACS Appl Mater Interfaces 9(6):5288–5294

41. Wu K, Liu D, Yun T (2018) In-situ single step chemical synthesis of graphene-decorated CoFe$_2$O$_4$ composite with enhanced Li ion storage behaviors. Electrochimica Acta: S0013468618300744